SAND2018-3879J

Design and Testing of a Magnetically Driven Implosion Peak Current Diagnostic

M. H. Hess, ^{1,*} K. J. Peterson, ¹ D. J. Ampleford, ¹ B. T. Hutsel, ¹ C. A. Jennings, ¹ M. R. Gomez, ¹ D. H. Dolan, ¹ G. K. Robertson, ¹ S. L. Payne, ² W. A. Stygar, ¹ M. R. Martin, ¹ and D. B. Sinars ¹

¹Sandia National Laboratories, Albuquerque, New Mexico 87185 ²National Security Technologies, LLC, Albuquerque, New Mexico 87185 (Dated: April 11, 2018)

A critical component of the magnetically driven implosion experiments at Sandia National Laboratories is the delivery of high-current, 10's MA, from the Z pulsed power facility to a target. In order to assess the performance of the experiment, it is necessary to measure the current delivered to the target. Recent Magnetized Liner Inertial Fusion (MagLIF) experiments have included velocimetry diagnostics, such as PDV (Photonic Doppler Velocimetry) or VISAR (Velocity Interferometer System for Any Reflector), in the final power feed section in order to infer the load current as a function of time. However, due to the nonlinear volumetrically-distributed magnetic force within a velocimetry flyer, a complete time-dependent load current unfold is typically a time-intensive process, and the uncertainties in the unfold can be difficult to assess. In this paper, we discuss how a PDV diagnostic can be simplified to obtain a peak current by sufficiently increasing the thickness of the flyer. This effectively keeps the magnetic force localized to the flyer surface resulting in fast and highly accurate measurements of the peak load current. In addition, we show the results of experimental peak load current measurements from the PDV diagnostic in recent MagLIF experiments.

I. INTRODUCTION

The Sandia National Laboratories MagLIF platform [1] utilizes approximately 20 MA from the Z pulsed power machine [2] to implode a laser-preheated, deuteriumfilled metallic liner that is approximately 3 mm in radius and less than 1 cm in length at speeds of around The MagLIF liner acts as a Z-pinch and compresses the deuterium fuel to thermonuclear conditions through near-adiabatic compression [3]. Velocimetry measurements using either VISAR (Velocity Interferometer System for Any Reflector) [4] or PDV (Photonic Doppler Velocimetry) [5] have been powerful tools in inertial confinement fusion [6] and equation-of-state [7, 8] research. In addition, velocimetry measurements of thin metallic flyer plates have been particular useful for diagnosing magnetic pressures and their associated load currents [9–13] in multi-MA pulsed power applications. In particular, Ref. 13 discusses an aluminum PDV diagnostic that is roughly 400 μ m thick and located 3 mm below a MagLIF target at a radius of 1.3 cm in the final power feed section. These diagnostics are significantly closer in proximity to the load than any other load current diagnostics, e.g. the closest Z-machine B-dot probes [14] are at a radius of 5.9 cm. However, it is well-known that B-dot probes can have limited performance with high inductance loads, such as MagLIF, due to various failure mechanisms [15]. Therefore, measuring the load current with PDV diagnostics offers the best inference of the actual current in the MagLIF load.

In general, however, the unfold process to obtain the time-dependent load current from the PDV velocity data is a time-intensive process. For example, with typical MagLIF currents, one may be required to perform hundreds, or even thousands, of MHD simulations using different load currents to find a current whose corresponding simulated flyer velocity is within a few percent agreement of the experimental velocity data. The primary reason for the difficulty in the unfold process is that the magnetic fields, as well as the current that generates them, nonlinearly diffuse through the PDV diagnostic as a function of space and time. Therefore, the velocity that is measured by a PDV load current diagnostic will depend on the nonlinear spatially- and temporally-dependent $\mathbf{J} \times \mathbf{B}$ forces throughout the flyer volume. Additionally, it is often difficult to assess the uncertainty in a particular current unfold since two different current shapes can produce similar flyer velocities.

By simply increasing the aluminum flyer thickness to at least 600 μm , we reduce the magnetic field diffusion sufficiently over the 120 ns MagLIF current pulses, so that the distributed $\mathbf{J} \times \mathbf{B}$ forces in the aluminum are effectively kept near the flyer surface. In this regime, magnetic pressure driven flyer motion mimics that of a mechanical pressure driven flyer whose velocity is directly correlated to a pressure at an earlier time when the flyer does not exhibit a significant shock near the free flyer surface (see for example [16]). Therefore, a peak magnetic pressure, and hence peak load current, is directly related to a peak flyer velocity under certain conditions that will be discussed. This operational regime of the PDV diagnostic enables a fast and accurate peak load current measurement. Moreover, since there is a one-toone correlation between the measured peak flyer velocity and the inferred peak load current, we are able to estimate an uncertainty in the peak load current.

Our paper is organized as follows: in Sec. II we discuss the experimental configuration for the MagLIF PDV load current diagnostic, in Sec. III we show how design considerations yield a range of acceptable thicknesses for the diagnostic flyer and show experimental measurements

^{*}Electronic address: mhess@sandia.gov

from MagLIF shots, in Sec. IV we describe sources of uncertainty in our diagnostic and provide an estimate of the uncertainty in the measured peak load current for recent MagLIF shots, and in Sec. V we give a summary.

II. EXPERIMENTAL CONFIGURATION

The PDV load current diagnostic is located a few millimeters below the slotted return can as shown in Figure 1. The slotted return can is at the same axial height as the MagLIF load. Three dimensional simulations of the current flow at the PDV diagnostic's axial location indicate that the azimuthal variation of the current around the entire return can due to the 9 posts in the return can is less than 5 % [17]. The inner flyer surface is at a radius of 1.3 cm, and the flyer is 600 μ m thick and is made of aluminum-6061 alloy. The experimental setup is nearly identical to the one described in detail in Ref. 13, except that the flyer thickness in Ref. 13 was 384 μ m. For the relevant MagLIF current pulse length of 120 ns and peak load current in the range of 15-20 MA, the effects of magnetic diffusion on the flyer velocity can be significant for the 384 μ m thick flyer, but are relatively small for the 600 μ m thick diagnostic in the present paper. Specifically, simulations show that the $\mathbf{J} \times \mathbf{B}$ force density for the 600 μ m thick diagnostic at the time of peak current is limited to roughly 30% of the flyer mass closest to the drive current with the dominant portion of the force density in the 10-20% of the mass closest to the drive current. In comparison, the $\mathbf{J} \times \mathbf{B}$ force density for the 384 μ m thick diagnostic is distributed throughout roughly 50% of the flyer mass at the time of peak current.

This is clearly seen in Figure 2, in which we plot the radial component of the $\mathbf{J} \times \mathbf{B}$ force density for both a $600 \mu m$ and a 384 μm flyer at five flyer positions corresponding to 10%, 20%, 30%, 40%, and 50% of the flyer mass as measured from the inner flyer edge where the magnetic pressure is applied. In general, the magnetic diffusion process through the flyer is quite complicated, and includes important physics, such as local melting and hence, a rapid increase in the local resistivity which is seen in the small sharp peaks of Fig. 2. By increasing the flyer thickness, we are effectively keeping the complicated physics of magnetic diffusion more localized to the flyer surface. These flyer simulations and subsequent simulations in this paper were performed using the arbitrary-lagrangian-eulerian multimaterial code, ALEGRA [18], developed at Sandia National Laborato-

A primary assumption in designing the peak current diagnostic is that the current pulse should rise to a single peak at some point in time, and the width of the current pulse near the peak should be sufficiently large such that a rarefaction wave will not overtake the stress wave in the flyer induced by the peak magnetic pressure. When an unloading process occurs after peak pressure is achieved in a solid, it is well-known that the rarefaction waves corresponding to the unloading process can overtake the peak pressure after a sufficient period of time [19]. As

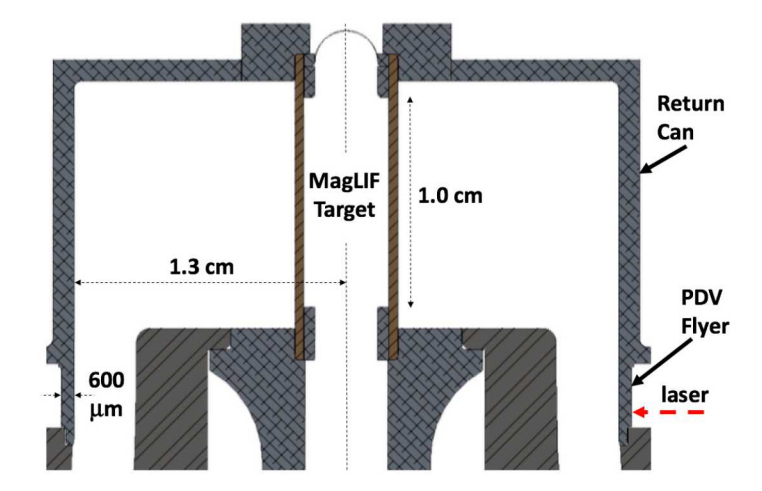


FIG. 1: Illustration showing the location of the PDV load current diagnostic in relation to the return can.

an example of a current pulse which meets our primary assumption, Figure 3 shows a plot of the load current for MagLIF shot Z2850 (red) with a peak of 18.3 MA, which is produced using the BERTHA [20] circuit code in conjunction with a model of the Z machine developed at Sandia [21]. Figure 3 also shows a simulation of a 600 μ m flyer velocity (red) for the Z2850 circuit current. As the MagLIF target is compressed until stagnation (which occurs 10's ns after peak current), the inductance of the load increases and the current rolls over at a quicker rate than the rise rate. However, the current pulse width near the peak of Z2850 is sufficiently large to produce a smooth flyer velocity near the peak for the 600 μ m flyer.

III. DIAGNOSTIC DESIGN AND EXPERIMENTAL MEASUREMENT

Since we don't know the precise current shape prior to a MagLIF experiment, then it is essential that the peak load current diagnostic should be relatively insensitive to the current pulse shape. That is, for currents that have rise times of around 120 ns and peaks with similar widths, one should produce the same peak flyer velocity (up to a small error) for the same peak current regardless of the current shape. In order to test the performance of the diagnostic through simulation with different current shapes, we introduce a time-dependent Lorentzian current model which has three adjustable parameters, the peak current I_{peak} , the time of peak current t_{peak} , and peak width Δt . Specifically,

$$I(t) = \frac{I_{peak}}{1 - f(t_{peak})} (f(t - t_{peak}) - f(t_{peak})) , \qquad (1)$$

where

$$f(t) = \frac{1}{1 + t^2/\Delta t^2} \ . \tag{2}$$

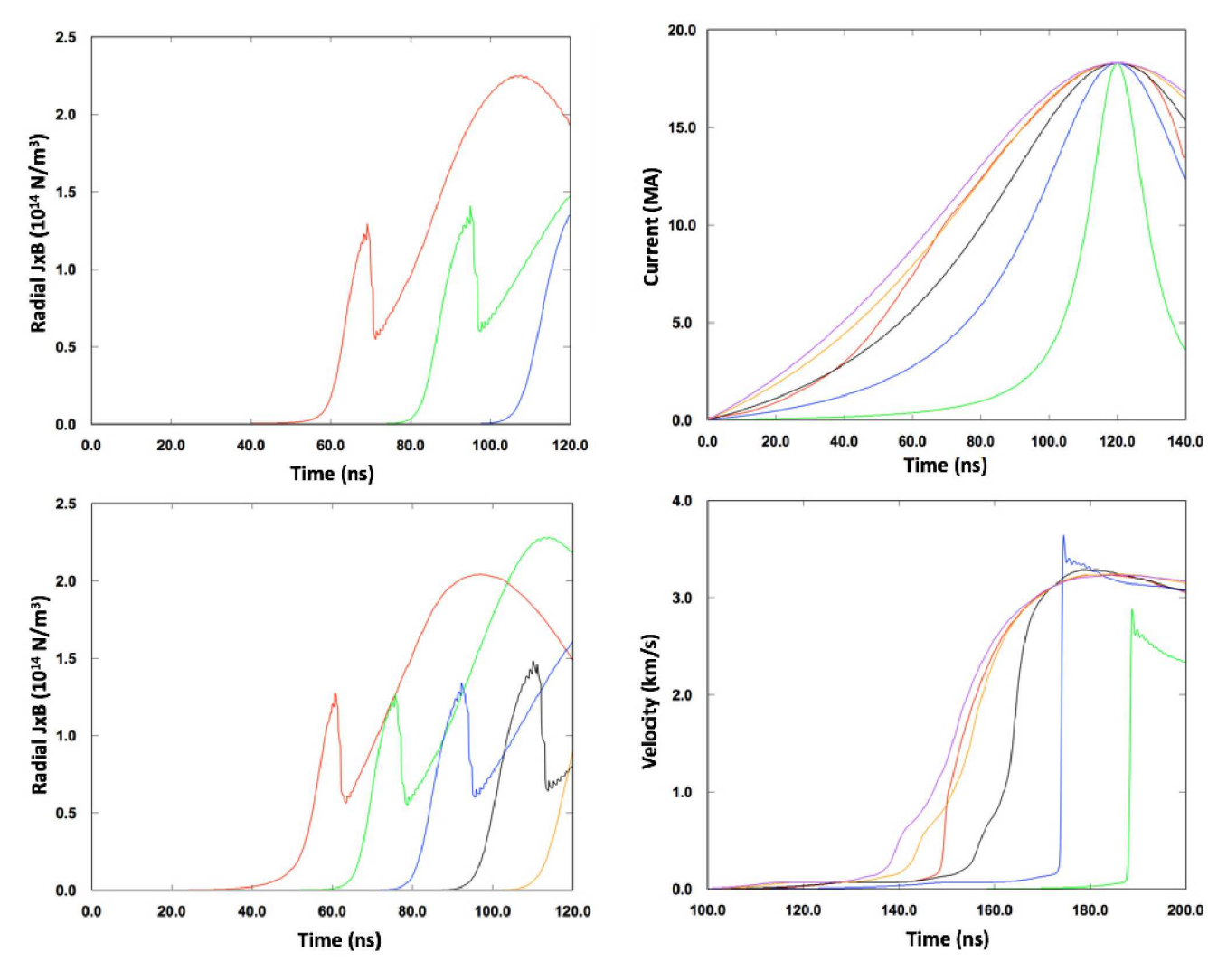


FIG. 2: Plots of radial $\mathbf{J} \times \mathbf{B}$ force densities for a 600 μ m flyer (top) and a 384 μ m flyer (bottom) at positions of 10% (red), 20% (green), 30% (blue), 40% (black), and 50% (orange) of the flyer mass as measured from the inner flyer edge.

FIG. 3: Plots of load currents (top) and simulated flyer velocities (bottom): Z2850 circuit model (red), model with $\Delta t = 10$ ns (green), model with $\Delta t = 30$ ns (blue), model with $\Delta t = 50$ ns (black), model with $\Delta t = 70$ ns (orange), and model with $\Delta t = 80$ ns (purple).

Figure 3 shows plots of model currents with the same peak current and location of peak current as Z2850 (I_{peak} = 18.3 MA and t_{peak} = 120 ns), but with different widths near the peak, i.e. $\Delta t = 10$ ns (green), 30 ns (blue), 50 ns (black), 70 ns (orange) and 80 ns (purple). Fig. 3 also shows plots of the simulated flyer velocities for each load current. Table I shows the simulated peak velocities for different load current models. We find, in general, that wider current peaks tend to have a smaller peak velocity variation compared to the smaller current peaks. This is due to two effects: 1) a wider current peak does not cause shocking near the peak velocity and 2) a wider current peak delays the time for the pressure release wave to erode into the peak pressure wave within the flyer before it reaches the flyer surface. Since the peak current diagnostic is using the peak velocity of the flyer to infer the peak magnetic pressure, and hence the peak current,

it is necessary to prevent the merging of wave characteristics, i.e. shock buildup, on the free flyer surface near the time of peak velocity. Shock buildup near the time of peak velocity can occur when faster moving pressure waves that are emitted from the magnetic pressure surface at later times combine with slower moving pressure waves that are emitted at an earlier time. Prevention of shock buildup near the time of peak velocity becomes an important design consideration which we discuss later.

The largest difference in simulated peak velocities in the wider peak width range of 50 ns $\leq \Delta t \leq 80$ ns is 1.5%. However, as the peak width is decreased to $\Delta t = 30$ ns, the velocity profile near the peak velocity shows a strong shock, and the difference in the peak is 12.6%. The shock feature is exactly correlated with a sharp increase in the flyer density near the free flyer surface at the time of

Current Model	Peak Velocity (km/s)
Z2850 Circuit	3.237
$\Delta t = 10 \text{ ns}$	2.879
$\Delta t = 30 \text{ ns}$	3.644
$\Delta t = 50 \text{ ns}$	3.286
$\Delta t = 70 \text{ ns}$	3.242
$\Delta t = 80 \text{ ns}$	3.234

TABLE I: Comparison of simulated peak flyer velocities for different load current models.

the shocked peak velocity, which is approximately 16.3% greater than the initial flyer density. When shock buildup occurs near the free flyer surface, the density near the surface is larger resulting in a higher pressure, and hence, higher velocity. The inferred pressure from the shock will cause an overestimate of the magnetic pressure/load current that was applied at an earlier time to the flyer drive surface. Therefore, strong shocking near the time of peak velocity, such as in the $\Delta t = 30$ ns case, implies that the diagnostic is no longer operating in a regime where we can reliably relate the peak velocity to a corresponding peak magnetic pressure/peak current at an earlier time. As a comparison, the $\Delta t = 70$ ns case exhibits a very weak increase in the density at the free flyer surface near the time of peak velocity, i.e. only 0.6% compared to the initial density. Elimination of the shocking feature near the time of peak velocity is a design consideration which ultimately leads to a maximum thickness for the flyer as discussed later in Equation (7). As the peak width is decreased further to $\Delta t = 10$ ns, the velocity profile is also shocked, but the rarefaction wave has now overtaken the stress wave induced by the peak magnetic pressure and caused the velocity peak to be reduced by 11.1%.

One can see however in Figure 3, that the Z2850 circuit model is similar in rise to peak value as the $\Delta t = 70$ ns model, and is similar in drop off near the peak as $\Delta t =$ 50 ns. Hence, one would expect variations in velocity for currents that are similar to the Z2850 current, i.e. similar rise time, peak current, and peak width to be in the range of 1.5% provided there was no sudden shorting of the power flow upstream of the measurement. Therefore, the magnetic pressure at peak current, which provides the peak magnetic pressure, is strongly correlated with the local peak velocity point at a later time (accounting for the time-delay associated with the finite sound speed of the stress wave propagating through the metal flyer), and is essentially independent of current shape to within a small variation over a reasonable range of current shapes. Hence, we can utilize this diagnostic to infer peak current directly from the measured peak velocity.

Figure 4 shows a plot of the inferred peak MagLIF current as a function of peak flyer velocity in red. This curve was generated through a series of simulations, which multiplied the Z2850 current with a scale multiplier factor to vary the peak current. In order to illustrate how this diagnostic mimics the behavior of a mechanical pressure driven flyer, we have used the 1-D flyer velocity formula

from Ref. 16, which is a function of the applied pressure at a previous time, i.e.

$$v = 2 \int_{0}^{P} \frac{dP}{\rho(P)c(P)} , \qquad (3)$$

where the density, ρ , and the sound speed c are found using the room temperature (T=298 K) SESAME 3700 aluminum table [22]. This formula provides a peak velocity in response to a peak pressure, which we equate to the magnetic pressure at a radius of 1.3 cm, as shown in the blue curve in Figure 4. The two curves show excellent agreement even though the simple 1-D model (blue) does not include the effect of magnetic diffusion, which is fully included in the ALEGRA calculations (red). Using the red curve in Figure 4, one can diagnose the peak current for a MagLIF shot by simply measuring the peak PDV velocity. The practical benefit of this diagnostic is that it allows for a reliable and quick measurement of the peak current of a MagLIF experiment.

As we have just shown, the peak load current diagnostic acts similar to a mechanical pressure driven velocimetry measurement and can produce very similar peak velocities for current pulse shapes with identical peak currents that are within a certain range of a pulse shape. For MagLIF experiments on the Z machine, a 600 μ m thick aluminum flyer works well. We will now introduce equations which describe a range of thicknesses for metal flyers, which can be used for designing this diagnostic on other current pulse shapes at other pulsed power facilities.

The first design consideration is that the flyer needs to be thick enough to prevent significant magnetic diffusion from occurring over the time scale of the pulse. For example, if we make the characteristic magnetic diffusion time 10 times greater than the pulse length, we arrive at the design relation

$$L > 10(\tau_{pulse}\eta/\mu_0)^{1/2}$$
, (4)

where τ_{pulse} is the current pulse length, e.g. 120 ns for MagLIF, μ_0 is the permeability of free space, and η is the resistivity of the flyer, e.g. $\eta = 25 \text{ n}\Omega$ for aluminum. Eq. (4) yields a minimum flyer thickness of roughly 490 μ m.

The second design consideration is that we need the current pulse length to be sufficiently wide near the peak to prevent a shock from forming near the time of the peak velocity. We can see the onset of the shocking feature in Fig. 3 for the curve in blue with $\Delta t = 30$ ns. In the limit when $\Delta t << \tau_{pulse}$, we find that $I(t_{peak} - \Delta t) = I(t_{peak})/2$, i.e. the current at a time Δt earlier than the peak, is about half of the peak current. Let us denote the density of the flyer at the time of peak current, i.e. $t = t_{peak}$, as ρ_p and at the time of half-peak current, i.e. $t = t_{peak} - \Delta t$, as ρ_{hp} . Let us also denote the sound speed of the flyer at the time of peak current as c_p and at the

time of half-peak current as c_{hp} . The times it will take for pressure waves to propagate from the magnetic driven surface of the flyer to the free flyer surface at $t=t_{peak}$ and $t=t_{peak}-\Delta t$ are given by

$$\Delta t_p = \frac{\rho_0 L}{\rho_p c_p} \tag{5}$$

and

$$\Delta t_{hp} = \frac{\rho_0 L}{\rho_{h\nu} c_{h\nu}} \ . \tag{6}$$

where $\rho_0 = 2700 \ kg/m^3$ for aluminum and the ratio of the densities accounts for the compression of the flyer [16]. In order to prevent a pressure wave generated at $t = t_{peak}$ from catching up to a pressure wave generated at $t = t_{peak} - \Delta t$, we need to satisfy $\Delta t > \Delta t_{hp} - \Delta t_p$ or

$$L < \Delta t / \left(\frac{\rho_0}{\rho_{hp}c_{hp}} - \frac{\rho_0}{\rho_p c_p}\right). \tag{7}$$

For a peak pressure corresponding to a peak current of 18.3 MA at a radius of 1.3 cm, we find roughly that $\rho_{hp}=2950~kg/m^3$, $\rho_p=3460~kg/m^3$, $c_{hp}=6030~m/s$, and $c_p=7470~m/s$. If we use, $\Delta t=50~\rm ns$ in Eq. (7) as the lower limit of Δt for MagLIF pulse shapes, then we arrive at a maximum thickness of about 1.0 mm. The reader should note that if we use $\Delta t=30~\rm ns$ in Eq. (7), then we arrive at a flyer thickness of roughly 600 μm . This is in agreement with the observation of the $\Delta t=30~\rm ns$ current profile having a velocity profile with a shock forming near the peak as shown in Fig. 3. For pulsed power machines that produce current profiles with a FWHM similar to or less than $\Delta t=30~\rm ns$, one would need to decrease the thickness of the flyer enough to satisfy Eq. (7), while still maintaining enough flyer thickness to satisfy Eq. (4).

Figure 5 shows a plot of the experimentally measured PDV flyer velocity for MagLIF shots Z3018 (red), Z3074 (green), Z3075 (blue), and Z3076 (black). All four of these shots featured beryllium liners that were 10 mm in height, but had different radii. In particular, Z3018 had an outer radius of 2.616 mm and an aspect ratio, $AR = r_{outer}/(r_{outer} - r_{inner}) = 9$, Z3074 had an outer radius of 3.400 mm with a 70 μ m plastic coating [23] and a mass matched AR = 11, Z3075 had an outer radius of 2.567 mm with a 75 μ m plastic coating and a mass matched AR = 9, and Z3076 had an outer radius of 3.400 mm with a 70 μ m plastic coating and a mass matched AR = 11. In Table II, we present the measured peak velocities and the peak load currents for each MagLIF shot. As a comparison, our BERTHA circuit model [21] for each of these shots predicts a peak current of 15.2 \pm $0.8 \text{ MA}, 17.9 \pm 0.9 \text{ MA}, 15.2 \pm 0.8 \text{ MA}, \text{ and } 18.5 \pm 0.9$ MA, respectively. The estimated uncertainty of the peak current predicted by the circuit model is roughly 5%.

IV. UNCERTAINTY ESTIMATES

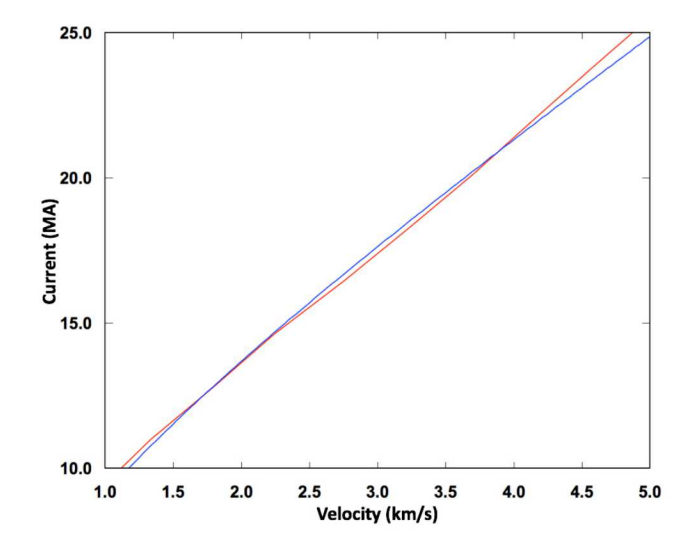


FIG. 4: Plot of the peak current inferred from the peak flyer velocity using ALEGRA simulations (red) and a 1-D model (blue).

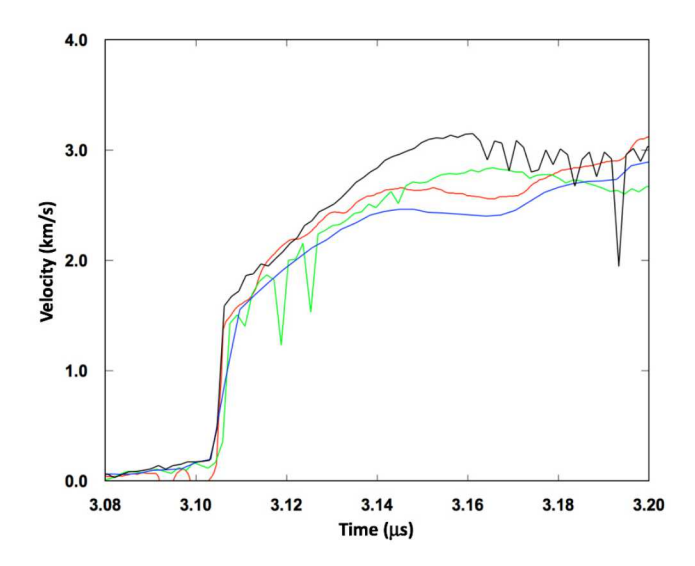


FIG. 5: Plots of measured PDV flyer velocities for MagLIF shots Z3018 (red), Z3074 (green), Z3075 (blue), and Z3076 (black).

In this section, we provide estimates of the uncertainty in the peak load current measurement provided by the PDV diagnostic. Sources of uncertainty for this diagnostic can be divided into two categories: 1) the uncertainty in the measurement of the peak velocity of the flyer with the PDV diagnostic and 2) variability in the simulated peak velocity for different current shapes, as well as, uncertainties in the equation-of-state and conductivity models. Our method for providing a total uncertainty on the peak current is a three step process. First, we provide estimates on the uncertainty and/or variability of the peak velocity from all known sources of uncertainty and/or variability. Then we calculate a total uncertainty on the peak velocity by adding all of these sources of un-

MagLIF Shot	Peak Velocity	I_{peak} (MA)
	$(\mathrm{km/s})$	
Z3018	2.638	16.0
Z3074	2.822	16.7
Z3075	2.435	15.2
Z3076	3.080	17.7

TABLE II: Measured peak velocities and peak currents for MagLIF shots.

certainty and/or variability in quadrature. Finally, using the peak velocity vs. peak current curve (red) in Fig. 4, we can estimate the peak current uncertainty from the total velocity uncertainty.

We estimate the uncertainty in the measured velocity v_{meas} , and denote its corresponding uncertainty as δv_{meas} . We know that there is a minimum uncertainty of the velocity signal as measured by the PDV diagnostic of \pm 10 m/s [12]. However, as seen from Fig. 5, the PDV velocity signal will have fluctuations near the local peak, which can exceed this minimum uncertainty. Our current practice in determining the peak velocity and its associated uncertainty is to find the local peak velocity in the signal, and then average over all velocities in a small time window, e.g. ± 3 ns, about the peak. The quoted peak velocity is the mean average over the time window, and the uncertainty is the standard deviation over the time window. For MagLIF shots, this typically yields uncertainties in the range $\pm 10\text{-}100 \text{ m/s}$, which for typical peak velocities yields fractional uncertainties in the range of $\delta v_{meas}/v_{meas}=0.5$ - 3.5%. The uncertainties in the peak velocities for MagLIF shots Z3018, Z3074, Z3075, and Z3076 are 15 m/s ($\delta v_{meas}/v_{meas} = 0.6\%$), 14 m/s ($\delta v_{meas}/v_{meas}=0.5\%$), 15 m/s ($\delta v_{meas}/v_{meas}=$ 0.6%), and 98 m/s ($\delta v_{meas}/v_{meas} = 3.2\%$), respectively.

In the second category, which uses simulation to model the flyer velocity for a given current, we can divide uncertainty into several subcategories: 1) the fluctuations in the simulated velocity near the peak, 2) variations in the peak velocity due to typical variations in the current shape, 3) variations in the peak velocity due to uncertainty in the equation of state table, 4) variation in the peak velocity due to uncertainty in the conductivity model. We find that in our typical ALEGRA simulations of the PDV diagnostic, fluctuations in the simulated velocity yield an uncertainty of about $\delta v_{fluc} = \pm 3$ m/s. These fluctuations could possibly be attributed to numerical noise in the simulations. In order to estimate the uncertainty due to shape variation in the current, we note that MagLIF current shapes are typically well constrained by the current shapes denoted by the $\Delta t = 50$ ns and $\Delta t = 80$ ns shown in Fig. 3. From Table I, we can immediately estimate the uncertainty in the peak velocity due to different current shapes as $\delta v_{shape} = \pm 50$ m/s.

We can estimate the uncertainty in the peak velocity from uncertainties in the equation of state table by applying a uniform uncertainty $P(\rho) = P_{true}(\rho)(1+\epsilon)$ to

Peak Velocity	$\delta v_{EOS}/v$	$\delta v_{cond}/v$
(km/s)	$(\epsilon=5\%,10\%)$	$(\epsilon=5\%,10\%)$
2.0	1.8%, 3.4%	0.2%,0.5%
3.0	1.5%, 2.8%	0.2%,0.4%
4.0	1.3%, 2.3%	0.4%, 0.7%

TABLE III: Comparison of estimated fractional peak velocity uncertainties for two different EOS and electrical conductivity uncertainties.

the EOS table, where P_{true} is the correct flyer EOS and ϵ is the uniform uncertainty, and then calculating the variation in the velocity from Eq. 3. The second column in Table III shows the fractional variation in the peak velocity due to uniform uncertainties of $\epsilon = 5\%$ and 10% in the aluminum EOS. We assume that this velocity variation is an additional uncertainty in the peak velocity, which will be used to calculate the final uncertainty in the peak current. It should be noted that our assumption of 5% uncertainty in the EOS is a conservative uncertainty estimate based on published shock Hugoniot data for aluminum-6061 [24].

Finally, we estimate the fractional uncertainty in the peak velocity for a given uncertainty in our electrical conductivity model. In our ALEGRA simulations, we use the Lee-More-Desjarlais (LMD) conductivity model [25] for aluminum. In a similar way for our uncertainty estimate in the EOS, we apply a uniform uncertainty to the electrical conductivity, i.e. $\sigma(\rho,T) = \sigma_{true}(\rho,T)(1+\epsilon)$. The third column in Table III shows the variation in the peak velocity as computed from the ALEGRA simulations assuming uniform uncertainties of $\epsilon = 5\%$ and 10% in the electrical conductivity model. It is apparent from Table III that the variation in the peak velocity for electrical conductivity uncertainties in the range of $5\% < \epsilon <$ 10% is weaker than the variation in the peak velocity for the same range of uncertainties on the EOS. For the present data, electrical conductivity uncertainties in the range of $5\% < \epsilon < 10\%$ produce a negligible effect on the total uncertainty in the peak current. Nevertheless, this uncertainty is included for calculating the final uncertainty in the peak current.

We now estimate the total uncertainty in the peak velocity from all known uncertainties, i.e. PDV peak velocity measurement uncertainty, fluctuations in the simulated peak velocity, peak velocity variation due to current shape variation, peak velocity uncertainty due to an EOS uncertainty, and peak velocity uncertainty due to an electrical conductivity uncertainty. Since we are estimating the uncertainties in the EOS and conductivity using a known uniform uncertainty shift, we categorize these two uncertainties as systematic. The other three uncertainties we categorize as random. We estimate the total uncertainty in the peak velocity by adding the systematic uncertainties in quadrature, and then combining the random uncertainties and the systematic uncertainties in quadrature [26, 27]. The total systematic uncertainty due

MagLIF Shot	$I_{circuit} \pm \delta I_{circuit}$	$I_{meas} \pm \delta I_{meas}$
	(MA)	(MA)
Z3018	15.2 ± 0.8	16.0 ± 0.3
Z3074	17.9 ± 0.9	16.7 ± 0.3
Z3075	15.2 ± 0.8	15.2 ± 0.3
Z3076	18.5 ± 0.9	17.7 ± 0.5

TABLE IV: Comparison of the measured peak currents with EOS uncertainties of 5%, as well as electrical conductivity uncertainties of either 5% or 10%, and the peak currents predicted from the circuit model assuming 5% uncertainty for MagLIF shots.

to uncertainties in the EOS and conductivity is given by

$$\delta v_{sys} = \sqrt{\delta v_{EOS}^2 + \delta v_{cond}^2} , \qquad (8)$$

and the total uncertainty in the velocity is given by

$$\delta v_{tot} = \sqrt{\delta v_{meas}^2 + \delta v_{fluc}^2 + \delta v_{shape}^2 + \delta v_{sys}^2} \ . \tag{9}$$

Finally, we can estimate the uncertainty in the peak load current from the total uncertainty in the peak velocity. We note that the dependence on the peak current as a function of peak velocity for our peak current diagnostic is approximately linear and given by

$$I_{peak} = (4.0 \frac{MA}{km/s}) v_{meas} + 5.4 MA .$$
 (10)

Therefore, the uncertainty in the peak current for our diagnostic is given by

$$\delta I_{peak} = (4.0 \frac{MA}{km/s}) \ \delta v_{tot}. \tag{11}$$

Assuming that our EOS model has an uncertainty of 5%, and also assuming that the electrical conductivity models have either 5% or 10% uncertainty (both yield the same overall uncertainty in the peak current due to the weaker dependence of the peak velocity on the conductivity), then we can estimate our measured peak

current uncertainties for MagLIF shots Z3018, Z3074, Z3075, and Z3076. These uncertainties are shown in Table IV. As a comparison, one can see that the measured peak load currents from the diagnostic and the predicted peak load currents from the BERTHA circuit model for these shots are in agreement to within the combined uncertainty bounds of both the diagnostic and the circuit model.

V. SUMMARY

In this paper, we have introduced a novel peak load current diagnostic for the Z-machine multi-MA MagLIF experiments, which can quickly and accurately measure the peak load current in these experiments without performing a time-consuming nonlinear unfold process. This diagnostic was designed by increasing the thickness of our previous PDV flyers such that the magnetic field, and hence magnetic pressure, is kept closer to the surface of the flyer. The flyer motion behaves similarly to a mechanical pressure driven flyer, whose velocity at any point in time can be correlated to a pressure from a previous point in time. Hence, the peak magnetic pressure generated by the peak current corresponds to the peak flyer velocity. In addition, we demonstrated how this diagnostic is relatively invariant to practical MagLIF pulse shapes making it robust to uncertainties in the current shape. Moreover, we have also estimated the uncertainty in the measured peak load current. At present, we have found that the measured peak currents for the recent MagLIF shots discussed in this paper are in agreement with the BERTHA circuit model of our experiments to within the combined uncertainty bounds of the diagnostic and the circuit model.

M. Hess would like to thank G. Laity, R. Vesey, C. Ruiz, K. Cochrane, and A. Porwitzky of Sandia National Laboratories for their helpful discussions. Sandia National Laboratories is a multimission laboratory managed and operated by National Technology & Engineering Solutions of Sandia, LLC., a wholly owned subsidiary of Honeywell International, Inc., for the U.S. Department of Energy's National Nuclear Security Administration under contract DE-NA0003525. The views expressed in the article do not necessarily represent the views of the U.S. Department of Energy or the United States Government.

S. A. Slutz, M. C. Herrmann, R. A. Vesey, A. B. Sefkow, D. B. Sinars, D. C. Rovang, K. J. Peterson, and M. E. Cuneo, Phys. Plasmas 17, 056303, 2010.

^[2] M. K. Matzen, M. A. Sweeney, R. G. Adams, J. R. Asay, J. E. Bailey, G. R. Bennett, D. E. Bliss, D. D. Bloomquist, T. A. Brunner, R. B. Campbell, G. A. Chandler, C. A. Coverdale, M. E. Cuneo, J.-P. Davis, C. Deeney, M. P. Desjarlais, G. L. Donovan, C. J. Garasi, T. A. Haill, C. A. Hall, D. L. Hanson, M. J. Hurst, B. Jones, M. D. Knudson, R. J. Leeper, R. W. Lemke, M. G. Mazarakis, D. H. McDaniel, T. A. Mehlhorn, T. J. Nash,

C. L. Olson, J. L. Porter, P. K. Rambo, S. E. Rosenthal, G. A. Rochau, L. E. Ruggles, C. L. Ruiz, T. W. L. Sanford, J. F. Seamen, D. B. Sinars, S. A. Slutz, I. C. Smith, K. W. Struve, W. A. Stygar, R. A. Vesey, E. A. Weinbrecht, D. F. Wenger, and E. P. Yu, Phys. Plasmas 12, 055503, 2005.

^[3] M. R. Gomez, S. A. Slutz, A. B. Sefkow, D. B. Sinars, K. D. Hahn, S. B. Hansen, E. C. Harding, P. F. Knapp, P. F. Schmit, C. A. Jennings, T. J. Awe, M. Geissel, D. C. Rovang, G. A. Chandler, G. W. Cooper, M. E. Cuneo, A. J. Harvey-Thompson, M. C. Herrmann, M. H. Hess, O.

- Johns, D. C. Lamppa, M. R. Martin, R. D. McBride, K. J. Peterson, J. L. Porter, G. K. Robertson, G. A. Rochau, C. L. Ruiz, M. E. Savage, I. C. Smith, W. A. Stygar, and R. A. Vesey Phys. Rev. Lett **113**, 155003, 2014.
- [4] L. M. Barker and R. E. Hollenbach, J. Appl. Phys. 43, 4669, 1972.
- [5] O. T. Strand, D. R. Goosman, C. Martinez, and T. L. Whitworth, Rev. Sci. Instrum. 77, 083108, 2006.
- [6] D. H. Munro, P. M. Celliers, G. W. Collins, D. M. Gold, L. B. Da Silva, S. W. Haan, R. C. Cauble, B. A. Hammel, and W. W. Hsing, Phys. Plasmas 8, 2245, 2001.
- [7] M. D. Knudson, D. L. Hanson, J. E. Bailey, C. A. Hall, J. R. Asay, and W. W. Anderson, Phys. Rev. Lett. 87, 225501, 2001.
- [8] M. Koenig, A. Benuzzi-Mounaix, A. Ravasio, T. Vinci, N. Ozaki, S. Lepape, D. Batani, G. Huser, T. Hall, D. Hicks, A. MacKinnon, P. Patel, H. S. Park, T. Boehly, M. Borghesi, S. Kar, and L. Romagnani Plasma Phys. Control. Fusion 47, B441, 2005.
- [9] J.-P. Davis, C. Deeney, M. D. Knudson, R. W. Lemke, T. D. Pointon, and D. E. Bliss, Phys. Plasmas 12, 056310, 2005.
- [10] R. W. Lemke, M. D. Knudson, and J.-P. Davis, Intl J. Impact Eng. 38, 480, 2011.
- [11] M. R. Martin, R. W. Lemke, R. D. McBride, J. P. Davis, D. H. Dolan, M. D. Knudson, K. R. Cochrane, D. B. Sinars, I. C. Smith, M. Savage, W. A. Stygar, K. Killebrew, D. G. Flicker, and M. C. Herrmann, Phys. Plasmas 19, 056310, 2012.
- [12] D. H. Dolan, Rev. Sci. Instrum. 81, 053905, 2010.
- [13] M. H. Hess, B. T. Hutsel, C. A. Jennings, J. P. VanDevender, A. B. Sefkow, M. R. Gomez, P. F. Knapp, G. R. Laity, D. H. Dolan, D. C. Lamppa, K. J. Peterson, W. A. Stygar, and D. B. Sinars, Phys. Plasmas 24, 013119, 2017.
- [14] T. C. Wagoner, W. A. Stygar, H. C. Ives, T. L. Gilliland, R. B. Spielman, M. F. Johnson, P. G. Reynolds, J. K. Moore, R. L. Mourning, D. L. Fehl, K. E. Androlewicz, J. E. Bailey, R. S. Broyles, T. A. Dinwoodie, G. L. Donovan, M. E. Dudley, K. D. Hahn, A. A. Kim, J. R. Lee, R. J. Leeper, G. T. Leifeste, J. A. Melville, J. A. Mills, L. P. Mix, W. B. S. Moore, B. P. Peyton, J. L. Porter, G. A. Rochau, G. E. Rochau, M. E. Savage, J. F. Seamen, J. D. Serrano, A. W. Sharpe, R. W. Shoup, J. S. Slopek, C. S. Speas, K. W. Struve, D. M. Van De Valde, and R.

- M. Woodring, Phys. Rev. ST Accel. Beams 11, 100401, 2008.
- [15] D. V. Rose, D. R. Welch, C. L. Miller, R. E. Clark, E. A. Madrid, C. B. Mostrom, T. C. Wagoner, J. K. Moore, W. A. Stygar, J. E. Bailey, T. J. Nash, G. A. Rochau, and D. B. Sinars, Phys. Rev. ST Accel. Beams 13, 040401, 2010.
- [16] M. Hess, K. Peterson, and A. Harvey-Thompson, High Power Laser Science and Engineering 3, e22 2015.
- [17] C. A. Jennings, private communication, 2017.
- [18] A. C. Robinson, T. Brunner, S. Carroll, R. Drake, C. Garasi, T. Gardiner, T. Haill, H. Hanshaw, D. Hensinger, D. Labreche, R. Lemke, E. Love, C. Luchini, S. Mosso, J. Niederhaus, C. Ober, S. Petney, W. Rider, G. Scovazzi, O. Strack, R. Summers, T. Trucano, V. Weirs, M. Wong, and T. Voth, AIAA Paper No. 1235, 2008, p. 15204.
- [19] Y. B. Zel'dovich and Y. P. Raizer, Physics of Shock Waves and High-Temperature Hydrodynamic Phenomena, Dover Publications, Inc., Mineola, 2002, pp. 749-750.
- [20] D. D. Hinshelwood, Memorandum Report 5158, 1984.
- [21] B. T. Hutsel, P. A. Corcoran, M. E. Cuneo, M. R. Gomez, M. H. Hess, D. D. Hinshelwood, C. A. Jennings, G. R. Laity, D. C. Lamppa, R. D. McBride, J. K. Moore, A. Myers, D. V. Rose, S. A. Slutz, W. A. Stygar, E. M. Waisman, D. R. Welch, and B. A. Whitney, Phys. Rev. Accel. Beams 21, 030401, 2018.
- [22] K. S. Holian, Los Alamos Lab. Rpt. LA-10160-MS. 1984.
- [23] K. J. Peterson, T. J. Awe, E. P. Yu, D. B. Sinars, E. S. Field, M. E. Cuneo, M. C. Herrmann, M. Savage, D. Schroen, K. Tomilinson, and C. Nakhleh, Phys. Rev. Lett. 112, 135002, 2014.
- [24] M. D. Knudson, R. W. Lemke, D. B. Hayes, C. A. Hall, C. Deeney, and J. R. Asay, J. Appl. Phys. 94, 4420, 2003.
- [25] M. P. Desjarlais, Contrib. Plasma Phys. 41, 267, 2001.
- [26] J. R. Taylor, An Introduction to Error Analysis: The Study of Uncertainties in Physical Measurements, 2nd ed. (University Science Books, Sausalito, CA 1997), pp. 107
- [27] R. H. Dieck, Measurement Uncertainty: Methods and Applications, 4th ed. (The Instrumentation, Systems, and Automation Society, Research Triangle Park, NC, 2007), pp. 79.